Renormalization group and dynamical maps for the hierarchical tight-binding problem

D. Würtz,* T. Schneider, A. Politi,† and M. Zannetti‡
IBM Research Division, Zurich Research Laboratory, 8803 Rüschlikon, Switzerland
(Received 21 January 1988; revised manuscript received 17 October 1988)

A tight-binding model in one dimension with hierarchical potential strength is investigated. The problem is reduced to three equivalent recursive relations: (i) for characteristic polynomials, (ii) for a renormalization-group transformation, and (iii) for traces of transfer matrices. On this basis, the nature of the energy spectrum and the character of the wave functions is elucidated. The scaling properties are also analyzed in terms of the stability of fixed points, period two-cycles, and aperiodic solutions. For short chains, resistance and transmission are calculated as functions of system length and energy in view of experimental realizations.

I. INTRODUCTION

The one-dimensional Schrödinger equation with quasiperiodic potential has attracted considerable renewed interest,[1,2] leading to an intermediate case between the random potential with localized eigenfunctions and the periodic one with extended states. Moreover, the new ability to produce semiconductor heterostructures[3,4] with control of the growth of each layer allows experimental realization of such arrangement of barriers. Here, the one-dimensional Schrödinger equation models the properties of the heterostructure perpendicular to the layers.[3] Another important class of irregular deterministic potential structures is given by a hierarchical array of barriers. They also arise in the context of classical diffusion,[5] anomalous relaxation in spin glasses,[6,7,8] molecular diffusion on complex macromolecules,[9] computing structures,[10] etc. It is therefore useful to investigate the structure of the spectrum and the nature of the eigenfunctions in a tight-binding model with a suitable hierarchical arrangement of potential barriers. We hope that the results of these novel structures will lead to experimental realizations and to the observation of new phenomena. For a preliminary account of our work we refer to Ref. 11.

In Sec. II we characterize and specify the model, giving an introduction to the general properties of the spectrum. The problem is reduced to recursion relations for the characteristic polynomials. The characteristic function associated with a given product of transfer matrices is studied by deducing the energy dependence of the integrated density of states and the inverse localization length. Further information is obtained from the participation ratio. In Sec. III we follow a renormalization-group (RG) approach through an exact decimation procedure. The fixed points are discussed, evaluating the corresponding eigenvalues for the linearized RG transformation. They yield the scaling exponents at special energies for the integrated density of states and for the wave functions. Scaling allows derivation of a simple scheme for evaluating the ground-state energy and the top of the spectrum very accurately. In Sec. IV we analyze the problem in terms of a trace map for the transfer matrices. In addition, we discuss period-2 cycles and aperiodic and bandlike solutions of the trace map. Further, we derive exact expression for the whole transfer matrix, which allows discussion of the Euclidean norm and the resistance on a given sublattice. The properties on the real lattice are considered in Sec. V. For short chains up to 1000 sites, which are of interest for experimental realizations, we calculate the length and energy dependence of the transmission and resistance. Finally, in Sec. VI we summarize our main results.

II. GENERAL PROPERTIES OF THE MODEL AND ITS SPECTRUM

Our model is the one-dimensional tight-binding Schrödinger equation on a periodic spatial lattice labeled by the site index n. The Hamiltonian $\mathcal{H}$ of the system,

$$\mathcal{H}=\sum_n V_n|\rangle\langle n|-\sum_n(|n\rangle\langle n+1|+|n+1\rangle\langle n|)\ , \quad (2.1)$$

has local-site potentials V_n and constant nearest-neighbor hopping matrix elements which will be set to unity and define the energy scale. The Hamiltonian leads to the following recursion relation for the wave function ϕ_n:

$$\phi_{n+1}+\phi_{n-1}-(V_n-E)\phi_n=0\ . \quad (2.2)$$

For the potential strengths V_n we assume a hierarchical structure

$$V_n=U_0R^k\ , \quad (2.3)$$

where

$$k=\max\{l|n(\mathrm{mod}2^l)=0\} \quad (2.4)$$

denotes the level of hierarchy. Without loss of generality, we assume $U_0>0$. Depending on the magnitude of R, we can distinguish different situations, as illustrated in Fig. 1. For $R\geq 1$ the potential V_n is unbounded from above, while for $R<-1$ it is unbounded both from above and below. In all other cases it is $|V_n|\leq U_0$. More precisely, for $0<R<1$ the potential V_n is always restricted to values between 0 and U_0, whereas for $-1<R<0$, $-U_0R<V_n<U_0$ holds. Furthermore, there are three limit configurations: (a) $R=-1$, where V_n can assume

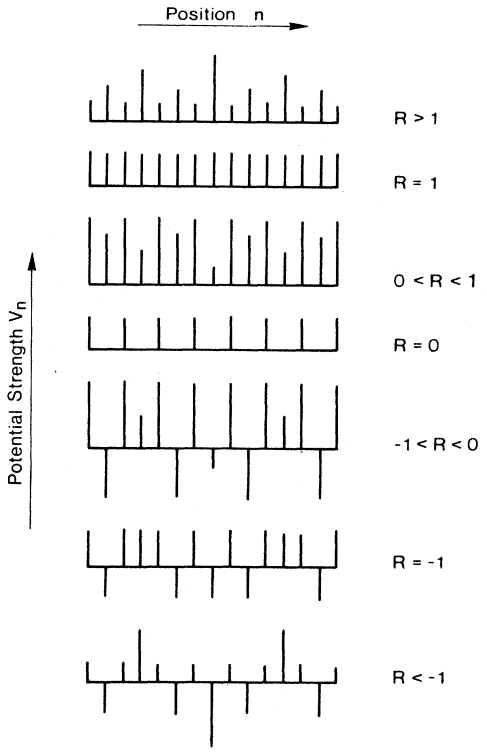

FIG. 1. Sketch of the hierarchical potential structures for a system of length $n=1,2,\ldots,15$ for various R values in Eq. (2.3).

two values only ($\pm U_0$) arranged in a special manner resembling Fibonacci superlattices; (b) $R=0$ and $R=1$, with a periodic potential V_n. $R=1$ is the completely ordered case where all $V_n=U_0$. $R=0$ describes a binary periodic potential, with $V_{2n+1}=U_0$ on odd and $V_{2n}=0$ on even sites.

The spectrum can be calculated by recurring to the matrix form of the Hamiltonian Eq. (2.1). The matrix $(\mathcal{H}-E)_{mn}$ is symmetric and tridiagonal with diagonal elements V_n-E and off-diagonal elements -1. The eigenvalues are the roots of the characteristic polynomial $P_n(E)$ satisfying the recursion relation

$$P_n(E)=(V_n-E)P_{n-1}(E)-P_{n-2}(E)\ , \tag{2.5}$$

with initial conditions $P_1(E)=U_0-E$ and $P_2(E)=P_1(E)(U_0R-E)-1$. The recursive relation (2.5) is formally equivalent to the initial Schrödinger equation (2.2), with ϕ_{n+1} corresponding to $P_n(E)$ with initial conditions $\phi_1=1$, $\phi_0=0$. This relationship will be further exploited in Sec. IV, deriving a recursive relation for the characteristic polynomial P_l of systems of length $n=2^l-1$. P_l satisfies

$$P_{l+1}(E)=2\tilde{P}_l(E)P_l(E)\ , \tag{2.6}$$

where $\tilde{P}_l(E)$ is of degree 2^l and satisfies the recursion relation

$$\tilde{P}_{l+1}=2(1+R)\tilde{P}_l^2+2R\tilde{P}_l-4R\tilde{P}_l\tilde{P}_{l-1}^2-1\ , \tag{2.7}$$

with initial conditions $\tilde{P}_0(E)=(U_0-E)/2$ and $\tilde{P}_1(E)=\tilde{P}_0(E)(U_0R-E)-1$. From Eqs. (2.6) and (2.7) it is seen that all eigenvalues of the 2^l-1 system remain eigenvalues of the $2^{l+1}-1$ system, and new eigenvalues are added which split off from the old ones, as indicated in Fig. 2. A more illustrative description of this eigenvalue tree is given in Fig. 3. As a function of the parameter R we have evaluated all ν eigenvalues $E_{l,\nu}$ for a system of size $n=2^l-1$. For $|R|>1$ the largest eigenvalue diverges ($\lim_{l\to\infty}E_{l,l}\to\infty$) and for $R<-1$ the lowest eigenvalue $E_{l,1}$ tends to minus infinity. The eigenvalue spectrum is thus bounded for $|R|\le 1$ only, when the potential V_n is bounded as well. Figure 3 also reveals a strong clustering of eigenvalues for $|R|\to\infty$. For large but finite $|R|$ values, the eigenvalues appear in groups merging for $|R|\to\infty$. Let us consider, as an example, the case $U_0=1$. For a system of size 2^l-1 we obtain l groups of eigenvalues $1\le\mu\le l$ with values $E_{l,\{\mu\}}\to R^{\mu-1}$ and multiplicity $2^{l-\mu}$. Thus, for $R=10$ and $l=7$ we obtain 64 eigenvalues around $E_{7,\{1,\ldots,64\}}\sim 1$, 32 eigenvalues around $E_{7,\{65,\ldots,98\}}\sim 10$, 16 eigenvalues around $E_{7,\{99,\ldots,114\}}\sim 100$, etc. Moreover, the special values $R=1$ and $R=0$ are accessible to an exact treatment. For $R=U_0=1$ (free particle) the eigenvalues are given by $E_\nu=3-4\sin^2(\nu\pi/2^{l+1})$, with $\nu=1,3,7,\ldots,2^l-1$. In the infinite system these eigenvalues form a continuous band $-1<E<3$ and the eigenstates are extended because $\lim_{N\to\infty}(1/N)\sum_{n=1}^{N}\phi_n^2=\text{const.}$ $R=0$ corresponds to the binary periodic potential $V_n=U_0/2[\cos(n-1)\pi+1]$. Setting $U_0=1$, there is a gap $(0<E<1)$ separating the two bands of extended states. The top and the bottom of the spectrum are given by $E=\frac{1}{2}(1\pm\sqrt{17})$.

For generic R values, however, the potential is no longer commensurate with the spatial periodicity of the lattice. Interesting features of the hierarchical potential structure can be anticipated by approximating it with periodic systems of increasing period. As it is doubled to reach the quasiperiodic limit, each band is split into subbands, finally leading to highly fragmented Cantor-like integrated density of states.[1,2] To confirm this expectation we have numerically evaluated the integrated density

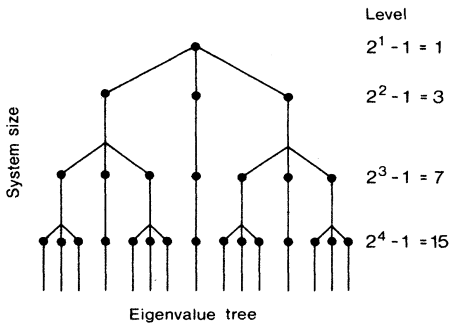

FIG. 2. Schmetic representation of the tree structure of the eigenvalues for system sizes $n=2^{l-1}$, $l=1,2,3,4$.

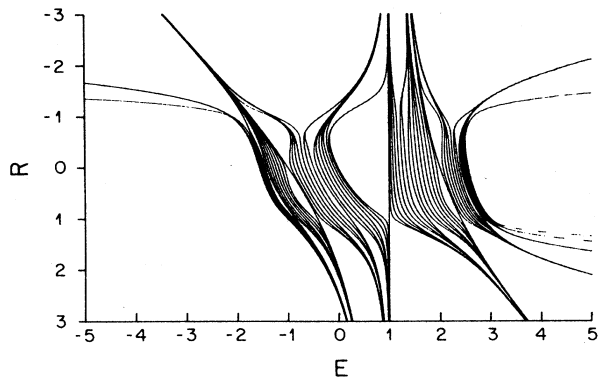

FIG. 3. R dependence of the eigenvalues for a system of size $2^6-1=63$.

of states $N(E)$, the exponential decay length $\gamma(E)$, and the participation ratio $\alpha(E)$. To do this, we define the ratio $\mathbf{R}_n$,

$$\mathbf{R}_n=\frac{\phi_n}{\phi_{n-1}} , \tag{2.8}$$

which allows rewriting of the Schrödinger problem as the nonlinear map

$$\mathbf{R}_{n+1}=V_n-E-\frac{1}{\mathbf{R}_n} . \tag{2.9}$$

The characteristic function $\Gamma(E)$ is then defined as

$$\Gamma(E)=\lim_{\epsilon\to 0}\Gamma(E+i\epsilon^+)=\lim_{N\to\infty}\frac{1}{N}\sum_{n=1}^{N}\ln\mathbf{R}_n . \tag{2.10}$$

Thus real and imaginary parts are given by

$$\begin{aligned}\mathrm{Re}\Gamma(E)&=\gamma(E)=\frac{1}{N}\sum_{n=1}^{N}\ln|\mathbf{R}_n| ,\\ \mathrm{Im}\Gamma(E)&=\tilde{\gamma}(E)=\pi\frac{1}{N}\sum_{n=1}^{N}\Theta(-\mathbf{R}_n)=\pi N(E) ,\end{aligned} \tag{2.11}$$

where $\Theta(x)$ is the unit step function, $\gamma(E)$ is the inverse exponential localization length, and $\tilde{\gamma}(E)$ corresponds to π times the density of negative, $\mathbf{R}_n's$; i.e., the density of modes of the wave function. So it is clear that $\tilde{\gamma}(E)$ equals π times the integrated density of states $N(E)$. In analogy with $\gamma(E)$, to cover cases where $\gamma(E)=0$, we introduce the algebraic localization length

$$\gamma_a(E)=\frac{1}{\ln N}\sum_{n=1}^{N}\ln|\mathbf{R}_n| . \tag{2.12}$$

It is important to emphasize that $\gamma(E)$ does not necessarily characterize localization of the wave function. In fact, $\gamma(E)$ is also finite in gaps where the wave function grows exponentially.

Another useful parameter characterizing the nature of the wave functions is the participation ratio $\alpha(E)$:

$$\alpha(E)=\lim_{N\to\infty}\frac{\left[\sum_{n=1}^{N}|\phi_n|^2\right]^2}{N\sum_{n=1}^{N}|\phi_n|^4} . \tag{2.13}$$

It measures the number of sites which effectively contribute to the eigenstate amplitude. If all sites equally participate, α becomes constant, whereas if only few sites participate, α tends to zero with increasing chain length N. In the quasiperiodic case the participation ratio allows distinction between exponentially localized states and power-law localized or extended states only. In the latter cases α tends to a constant. Thus, extended and algebraically localized states cannot be distinguished.

The expectation of a fragmented Cantor set, like the integrated density of states $N(E)$, is fully confirmed by numerical results for $N(E)$. Three typical examples for $N(E)$, as obtained from Eq. (2.11) by counting nodes, are shown in Fig. 4 for $U_0=1$. Here we also induced the inverse exponential localization length $\gamma(E)$ and the participation ratio $\alpha(E)$. Large gaps are readily identified at energy intervals where $N(E)$ is constant, $\gamma(E)$ large, and $\alpha(E)$ small. From the R dependence of the eigenvalue spectrum shown in Fig. 3, one expects fundamentally different behavior for $R>1$, $|R|\le 1$, and $R<-1$. Figure 4(a) illustrates the characteristic behavior for $R>1$. In analogy with the potential, top of the spectrum is un-

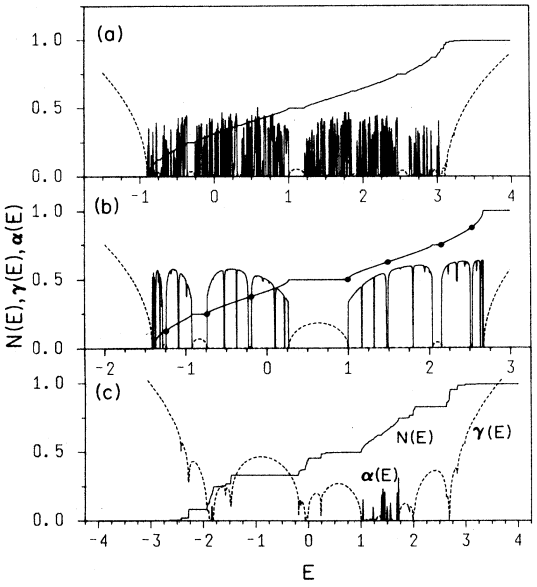

FIG. 4. Integrated density of states $N(E)$, inverse localization length $\gamma(E)$, and participation ratio $\alpha(E)$ for $U_0=1$ and a system of length $N\sim 10^6$ on an equally spaced energy grid of 1000 points. The seven dots mark the eigenvalues of a system of size 2^3-1, corresponding to the third level on the eigenvalue tree. (a) corresponds to $R=1.1$, (b) to $R=\sqrt{2}-1$, and (c) to $R=-1.1$.

bounded. The *rough* structure of the participation ratio and the localization length suggests the existence of exponentially localized states between the visible gaps. This turns out to be (Sec. IV) a consequence of numerical inaccuracy. In fact, no exponentially localized states exist. For $|R|<1$, the spectrum is unbounded from above and below, and the result presented in Fig. 4(b) suggests an almost continuous behavior. For further clarification we refer to the next section. Figure 4(c) shows an example for $R<-1$. Here, the bottom and the top of the spectrum are unbounded. Compared to the previous results for $R>0$, and those depicted in Figs. 4(a) and 4(b), the fragmentation of $N(E)$ is much more pronounced. This behavior reflects the clustering of the eigenvalues for $R<-1$. Another interesting feature appears at energy $E=1$, which belongs to the spectrum for any R, provided that $V_0=1$ (see next section). For $R>1$ there is a gap above $E=1$, for $R=1$ the gap is removed and reappears below $E=1$ for $-1\le R<1$. For $R<-1$ it is again removed. Indications of this behavior can be anticipated from the R dependence of the eigenvalues shown in Fig. 3. The dots in Fig. 4 mark energies belonging to the eigenvalues tree, shown in Fig. 2 for a system of size 2^3-1. These energies seem to mark gap orders. To substantiate this expectation, we note that gaps can be labeled by integers $p=1,\ldots,2^l-1$ and the fraction $N(E)$ below gap p is $p/(2^l-1)$.

For a more qualitative characterization of the fragmentation of $N(E)$ we turn to the fractal properties. For $|R|>1$ the problem is highly nontrivial, due to the unboundedness of the spectrum. First we notice that the standard box-counting algorithm is inapplicable, since an infinite number of boxes is required to cover the spectrum at any resolution level. On the other hand, a density of boxes per unit length be introduced, as the whole mass is finite $[N(\omega=\infty)=1]$. We must therefore consider boxes centered around points of the spectrum chosen at random. In this way we can associate a "local" dimension α to each box as

$$\alpha=\frac{\ln\rho}{\ln\epsilon}\ , \tag{2.14}$$

where ϵ is the ω width of the box and ρ is the fraction of eigenvalues belonging to such an interval. Even this refined approach, however, exhibits striking contradictions which confirm the anomalous properties of this fractal. Indeed, when using boxes with the same width to cover the upper tail of the spectrum, smaller and smaller masses ρ are detected, suggesting a diverging dimension [see Eq. (2.14)]. This result, however, is an artifact, since the true widths of the clusters of eigenvalues are increasingly thinner and the true dimension shrinks to 0. To our knowledge, this spectrum constitutes the first example of a fractal set, which can be properly analyzed only by using boxes with variable size (the width of the cluster) and variable mass.[12]

For $|R|<1$ no problems arise, as the spectrum is bounded. Figure 4(b) suggests the existence of an almost continuous structure. In the next section this expectation will be substantiated by showing that the spectrum is a so-called "fat" fractal, where the relative weight of the gaps vanishes with increasing resolution. Such a feature is analogous to Harper's equation,[1] exhibiting extended eigenfunctions for a certain range of potential strength. This conclusion is also strongly supported by the behavior of the exponential localization length and the participation ratio.

III. RENORMALIZATION-GROUP APPROACH

Since the problem involves a hierarchy of energy scales and has a self-similar structure, one expects an interpretation within the renormalization-group RG context to be useful. In doing so we implement an exact decimation, preserving the hierarchical structure. We eliminate all odd sites. The resulting RG transformation, with rescaling factor equal to 2, yields a Schrödinger equation for the even sites as

$$\phi_{2n+2}+\phi_{2n-2}-[V_{2n}(U-E)-(2-E^2+EU)]\phi_{2n}=0\ . \tag{3.1}$$

This equation has exactly the same form as Eq. (2.2), except for the parameters which have been changed. In place of the energy E, there appears $E'=2-E^2+EU$. Making use of the definition of the potential in the expression $V_{2n}(U-E)$, we obtain, in place of U, $U'=RU(U-E)$. These recursion relations can be interpreted in the following way: Given an eigenstate of a system of size $n=2^{l+1}-1$, there exists a corresponding solution with parameters E' and U' on the lattice with $n'=2^l-1$. Hence, the transformation can be written as a recursion relation,

$$E_{l+1}=2-E_l^2+E_lU_l,\quad U_{l+1}=RU_l(U_l-E_l)\ . \tag{3.2}$$

We have analyzed this map and evaluated the fixed points and the corresponding eigenvalues listed in Table I. The recursion relation can also be interpreted as a transfor-

TABLE I. Fixed points and eigenvalues of RG [Eq. (3.2)] and trace maps [Eq. (4.10)].

Fixed point no.	E^*	u^*	x^*	y^*	λ_1,λ_2
1	1	0	$-\frac{1}{2}$	0	$-2,-R$
2	-2	0	1	0	$4,2R$
3	$\frac{2R}{R-1}$	$\frac{1}{R}+\frac{2R}{R-1}$	$\frac{1}{2R}$	$1+\frac{1}{2R}-\frac{1}{2R^2}$	$1+\frac{1}{2R}\pm\left[\left[1+\frac{1}{2R}+R\right]^2-\frac{2}{R}\right]^{1/2}$

mation of the parameters $y=(E,U)$. For initial values y_0, belonging to the spectrum or corresponding to gap edges, the iterates remain bounded. Moreover, there are special E_0 values whose iterates lead to a fixed point. This behavior implies simple scaling properties. Let $E_0+\Delta E$ belong to the spectrum. The integrated density of states will then behave as

$$|N(E_0+\Delta E)-N(E_0)|\sim|\Delta E|^{\bar{x}}G(|\Delta E/|\lambda|_{\max}|)\ , \tag{3.3}$$

where the scaling exponent $\bar{x}$ is given by

$$\bar{x}=\frac{\ln 2}{\ln|\lambda|_{\max}}\ . \tag{3.4}$$

This scaling behavior is easily verified by considering $N(E_0+\Delta E)$ for systems of sizes $2^l, 2^{l-1}, \ldots$. For $E_0=1+\epsilon$ we obtain from Eq. (3.2) the recursion relation

$$\begin{aligned} N(1+\epsilon,U_0=1)&=\tfrac{1}{2}N(2-\epsilon,-R\epsilon)\\ &=\tfrac{1}{4}N(-2+2\epsilon(2-R),+R^2\epsilon)\\ &=\tfrac{1}{8}N(-2-8\epsilon(2-R)-4R^2\epsilon,-4R^3\epsilon)\\ &=\tfrac{1}{16}N(-2+32\epsilon(2-R)\\ &\qquad -8R^2\epsilon+8R^3\epsilon,-8R^4\epsilon)=\cdots\ . \end{aligned} \tag{3.5}$$

It is then easily seen that

$$\begin{aligned} N(1+\epsilon)-N(1)&\to\frac{1}{2^l}[N(-2\pm\epsilon|\lambda|^l_{\max})-N(-2)]\\ &=\frac{1}{2^l}[N(E^*\pm\epsilon|\lambda|^l_{\max})-N(E^*)]\ , \end{aligned} \tag{3.6}$$

where $|\lambda|_{\max}=4$ for $|R|\le 2$ and $|\lambda|_{\max}=2R$ for $|R|>2$, in agreement with Table I for fixed point no. 2. The scaling law Eq. (3.3) is then a solution of Eq. (3.6) and can be extended to other E_0 values belonging to the tree or leading to fixed point no. 3. Two examples of the scaling behavior are given in Fig. 5 for $U_0=1$, $R\sqrt{3}/3$, and $E_0=1+\sqrt{3}$, where the energy corresponds to the top of the spectrum. Since this energy leads to fixed point no. 3, we expect the scaling exponent to be $\bar{x}=0.498\ldots$ as confirmed by the numerical analysis. Moreover, the amplitude $G(|\Delta E/|\lambda|_{\max}|)$ appears to be periodic with period $\ln|\lambda|_{\max}$. The lower curve in Fig. 5 illustrates $N(E)$ for parameters $U_0=1$, $R=-0.5$, and $E_0=1$ leading to fixed point no. 2. The numerical results confirm the scaling prediction with $\bar{x}=\ln 2/\ln 4=\frac{1}{2}$.

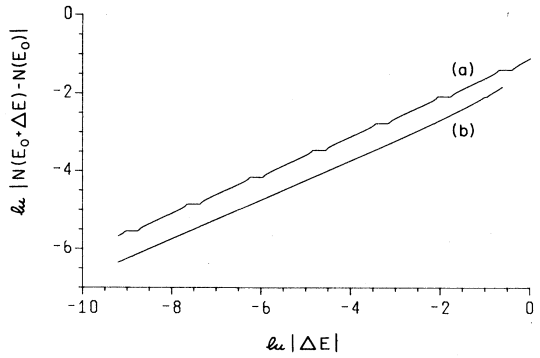

FIG. 5. In $|N(E_0+\Delta E)-N(E_0)|$ vs ln $|\Delta E|$ illustrating the scaling behavior [Eq. (3.3)], for (a) $R=\sqrt{3}/3$, $E_0=1+\sqrt{3}$, $U_0=1$ and (b) $R=-0.5$, $E_0=1$, $U_0=1$.

From the scaling behavior of the integrated density of states $N(E)$, the ground-state energy $E_{\rm bot}$ and the top of the spectrum can be very accurately evaluated. For example, considering scaling at the bottom of the spectrum

$$\ln N(E-E_{\rm bot})=\ln c+\bar{x}\ln(E-E_{\rm bot})\ . \tag{3.7}$$

This equation has three unknown variables: c, $E_{\rm bot}$, and $\bar{x}$. Consider the eigenvalues $E_{l,\nu}$ with $\nu=1$, 2, and 4 for a system of size 2^l-1. Since we know $N(E_{l,\nu})$, we can eliminate c and $\bar{x}$ from Eq. (3.7) and find

$$E_{\rm bot}=\lim_{l\to\infty}\frac{E_{l,2}^2-E_{l,1}E_{l,4}}{2E_{l,2}-E_{l,1}-E_{l,4}}\ . \tag{3.8}$$

Similarly, we find for the top of the spectrum

$$E_{\rm top}=\lim_{l\to\infty}\frac{E_{l,l-1}^2-E_{l,l}E_{l,l-3}}{2E_{l,l-1}-E_{l,l}-E_{l,l-3}}\ . \tag{3.9}$$

The estimates for the ground-state energy $E_{\rm bot}$ and the top of the spectrum $E_{\rm top}$ obtained from these expressions are listed in Table II for some typical R values. For $R>1$, $E_{\rm top}$, and for $R<-1$, both $E_{\rm top}$ and $E_{\rm bot}$, are diverging, as they should be. Table II demonstrates that one can evaluate the values of $E_{\rm bot}$ and $E_{\rm top}$ with a precision of more than six digits from a very short system

TABLE II. Estimates of the ground-state energy $E_{\rm bot}$ and top of the spectrum $E_{\rm top}$ for different R values obtained from scaling arguments (3.8) and (3.9).

	$R=0$		$R=\sqrt{2}-1\approx 0.41\ldots$		$R+\frac{1}{3}\sqrt{3}\approx 0.57\ldots$		$R=1$	
l	$E_{\rm bot}$	$E_{\rm top}$	$E_{\rm bot}$	$E_{\rm top}$	$E_{\rm bot}$	$E_{\rm top}$	$E_{\rm bot}$	$E_{\rm top}$
5	−1.561 698	2.561 698	−1.414 324	2.669 230	−1.336 885	2.732 168	−1.000 125	3.000 125
6	−1.561 562	2.561 562	−1.414 220	2.669 053	−1.338 783	2.732 058	−1.000 008	3.000 008
7	−1.561 553	2.561 553	−1.414 214	2.669 036	−1.341 421	2.732 051	−1.000 000	3.000 000
8	−1.561 553	2.561 553	−1.414 214	2.669 034	−1.345 744	2.732 051		
9				2.669 034	−1.346 350			
∞	$\frac{1}{2}(1-\sqrt{17})$	$\frac{1}{2}(1+\sqrt{17})$	$-\sqrt{2}$			$1+\sqrt{3}$	−1	3
	−1.561 553	2.561 553	−1.414 214			2.732 051		

(approximately 500 sites long).

A similar scaling is also found for the spatial behavior of wave functions. For $U_0=1$ and E_0 values leading to a fixed point, the magnitude of the wave function grows algebraically on sites $n=2^l-1$:

$$|\phi(n)|\sim\alpha^{\bar{y}}\phi(n/\alpha)=\frac{|\lambda|_{\max}}{2}\phi(n/2)\sim n^{\bar{y}}\ , \tag{3.10}$$

where

$$\bar{y}=\frac{\ln(|\lambda|_{\max}|2)}{\ln 2}\ . \tag{3.11}$$

Note that Eq. (3.11) does not necessarily imply that the eigenfunction exhibits an algebraic growth rate $\bar{y}$ on all sites. In fact, we know from similar models (see Ref. 13) that other subsequences exist showing different (perhaps larger) exponents. Interesting considerations on the structure of the spectrum can be drawn from Eq. (3.2) for $R<1$. In such a case, we can reasonably conjecture that $|V_L|$ shrinks to 0 for $l\to\infty$. If this true, the RG map asymptotically reduces to the logistic map,[14]

$$E_{l+1}=2-E_l^2\ , \tag{3.12}$$

while the decay of U_l is given by

$$|U_n|=|E_{n-1}|\cdots|E_1||E_0||R|^{n-1}\ . \tag{3.13}$$

Accordingly, the evolution of U is completely determined by that of E. More precisely, being that the Lyapunov exponent of Eq. (3.12) is given by[14]

$$\sigma(E)=-\lim_{N\to\infty}\frac{1}{N}\sum_{l=1}^{N}\ln 2|E_l|=\ln 2\ , \tag{3.14}$$

it is immediately verified [substituting Eq. (3.14) in Eq. (3.13)] that a vanishing U_n is indeed consistent with the hypothesis $R<1$. For $R=1$, the RG map reduces exactly to the logistic map. Numerical evidence for the reduction to the logistic map is given in Fig. 6, showing E_{l+1} versus E_l for $R=-0.5$ and $E_0=1.01$.

Which initial conditions are attracted by the energy interval $[-2,2]$ remain to be seen. The basin of attraction is not a compact set, and escape is still possible, with a probability of less than 1. As a first step we note that the fixed point $(-2,0)$ lies on the border of the basin of attraction. In fact, any point $(-2-\epsilon,0)$ with $\epsilon>0$ escapes to infinity. The natural extension of this observation for $U=0$ leads to the conjecture that all points on the left of the second invariant manifold W_2 (the first being the E axis) escape, as shown in Fig. 7. Additionally, the backward iteration of the map allows all points on the right of the preimage W_2^{-1} of W_2 to escape as well. Note now that the whole straight line $U=E$ is mapped onto $(+2,0)$, which is on the border of the basin of attraction. It is therefore interesting to investigate what happens in the vicinity of this straight line. We start considering a horizontal segment $E=\bar{U}+\delta$. Its image is the parabola, written in a paramagnetic form as

$$E=2-\delta(\bar{U}+\delta),\quad U=-R\bar{U}\delta\ . \tag{3.15}$$

From Fig. 7 we see that a small portion of such a parabola lies on the right of W_2^{-1} and thus escapes. An estimate of its length is obtained from the crossing point between the parabola and W_2^{-1} which, in linear approximation, is given by

$$E=2+\frac{U}{2-R}\ . \tag{3.16}$$

The width δ is proportional to $\bar{U}$:

$$\delta=2\frac{R-1}{2-R}\bar{U}\ . \tag{3.17}$$

To investigate the structure of the spectrum around the $(n+2)$th preimage of the fixed point no. 2 we note that its nth iterate hits, be definition, the bisectrix $U=E$. Therefore, a small segment adjacent to that point will lie in the escaping sector. To estimate its length it is sufficient to analyze the behavior of such a segment during n iterations. From the logistic map we know that the initial length δ_0 is stretched by a factor 2^n ($\delta_0=2^n\delta$), while U_0 is contracted to $\bar{U}=R^nU_0$. Neglecting prefactors and substituting into Eq. (3.12) yields

$$\delta_0\sim\left[\frac{R}{2}\right]^n\ , \tag{3.18}$$

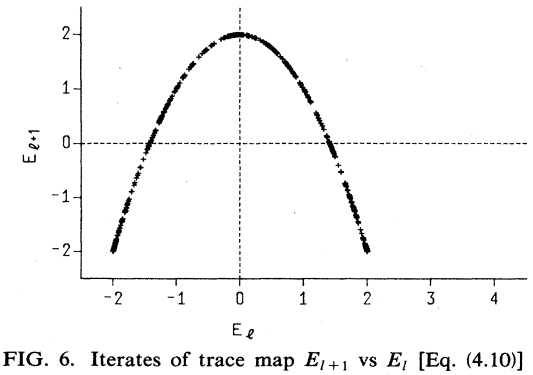

FIG. 6. Iterates of trace map E_{l+1} vs E_l [Eq. (4.10)] for a bandlike state with parameters $U_0=1$, $R=-0.5$, and $E=1.01$ for the first few hundred iterations.

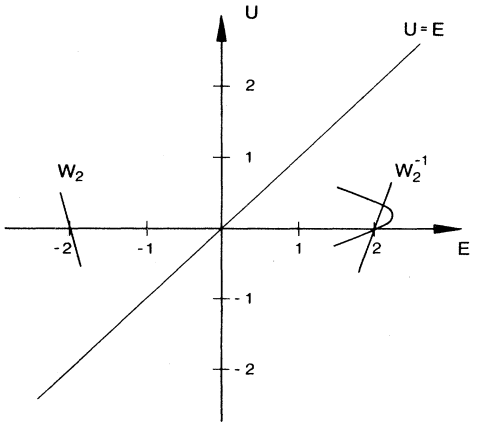

FIG. 7. Basin of attraction for the RG map [Eq. (3.2)]. The explanation is given in the text.

fixing the scale of the gaps in terms of n, the order of preimage. On the other hand, the width of the bands, whose number doubles with n, scales as $\delta_B = 2^{-n}$. Consequently, the ratio between gap and bandwidth shrinks to zero as

$$\frac{\delta_0}{\delta_B} \sim R^n . \tag{3.19}$$

Since the gaps disappear for $R < 1$, the fractal dimension tends to 1, and the spectrum is a so-called "fat" fractal with as strictly positive Lebesgue measure. In the derivation Eq. (3.19) we have implicitly assumed that no other invariant sets exist outside the line $U = 0$. This assumption is not correct. Indeed, there are particular energy values around which a standard fractal structure occurs. For $R = \sqrt{2} - 1$, the bottom of the spectrum, leading to fixed point no. 3, seems to be one of such points.

Most initial conditions, however, yield a dynamics which reduces to that of the logistic map. Therefore, since the maximum Lyapunov exponent is ln2 [see Eq. (3.14)], the algebraic exponent $\bar{\gamma}$ of the eigenfunction is 0 [Eq. (3.11)], indicating its extended nature.

IV. TRACE-MAP ANALYSIS

The problem can also be analyzed in terms of an iterative map for the transfer matrix. Referring to a finite sequence of length $n = 2^l$, Eq. (2.2) can be rewritten as

$$\begin{bmatrix} \phi_{2^l+1} \\ \phi_{2^l} \end{bmatrix} = \mathbf{M}^l \begin{bmatrix} \phi_1 \\ \phi_0 \end{bmatrix} , \tag{4.1}$$

where

$$M^l = \prod_{2^l}^{n=1} \begin{bmatrix} V_n - E & -1 \\ 1 & 0 \end{bmatrix} \equiv \prod_{2^l}^{n=1} T^n . \tag{4.2}$$

By noticing that the two subchains of length 2^l composing the chain of length 2^{l+1} are equal except for the last barrier, it is possible to derive

$$\mathbf{M}^{l+1} = (\hat{1} + \Lambda_l \hat{\mathbf{I}})(\mathbf{M}^l)^2, \quad \Lambda_{l+1} = R\Lambda_l , \tag{4.3}$$

where $\hat{1}$ is the 2×2 unit matrix and $\hat{\mathbf{I}}$ a 2×2 matrix whose elements are all zero except for $I_{12} = 1$, and the initial conditions become $M^0 = T^1$ and $\Lambda_0 = U_0(R-1)$. Rewriting Eq. (4.3) in the form

$$\mathbf{M}^{l+1} = (\hat{1} + \Lambda_l \hat{\mathbf{I}})\mathbf{M}^l[\mathbf{M}^l + (\mathbf{M}^l)^{-1}] - (\hat{1} + \Lambda_l \hat{\mathbf{I}}) , \tag{4.4}$$

and using the equality $\mathbf{M}^l + (\mathbf{M}^l)^{-1} = (\mathrm{Tr}\mathbf{M}^l)\cdot\hat{1}$ we can write a recursive relation for $x_l = \frac{1}{2}\mathrm{Tr}\mathbf{M}^l$:

$$x_{l+1} = 2x_l^2 + x_l\Lambda_l \mathrm{Tr}(\hat{\mathbf{I}}\mathbf{M}^l) - 1 . \tag{4.5}$$

Now we consider the relation for $\hat{\mathbf{I}}\mathbf{M}^l$:

$$\hat{\mathbf{I}}\mathbf{M}^{l+1} = 2x_l\hat{\mathbf{I}}\mathbf{M}^l - \hat{\mathbf{I}} , \tag{4.6}$$

and define

$$s_l = \tfrac{1}{2}\mathrm{Tr}(\hat{\mathbf{I}}\mathbf{M}^l) \equiv \tfrac{1}{2}\mathbf{M}^l_{21} . \tag{4.7}$$

Thus, we obtain

$$x_{l+1} = 2x_l^2 + 2x_l\Lambda_l s_l - 1, \quad s_{l+1} = 2x_l s_l . \tag{4.8}$$

By finally introducing the variable $y_l = 2x_l\Lambda_l$ we obtain the autonomous two-dimensional (2D) map

$$x_{l+1} = 2x_l^2 - 1 + y_l, \quad y_{l+1} = 2R_{x_{l+1}} y_l ; \tag{4.9}$$

or, by eliminating y_l,

$$x_{l+1} = 2(1+R)x_l^2 + 2Rx_l - 4Rx_l x_{l-1}^2 - 1 , \tag{4.10}$$

with initial conditions $x_1 = (U_0 - E)/2$, $x_2 = x_1(U_0 R - E) - 1$, and $y_1 = x_2 - 2x_1^2 + 1$. The equivalence with the RG map obtained in the previous section is an immediate consequence of the transformation $x_l = (U_l - E_l)/2$, $y_l = (R-1)U_l(U_l - E_l)$. The trace map is also related to the characteristic polynomial P_l. In fact, recalling the formal equivalent between P_l and ϕ_{2^l} with initial conditions $\phi_1 = 1$ and $\phi_0 = 0$, it is easily seen from Eq (4.1) that p_l is also equivalent to s_l, as seen in Eq. (4.7). As a consequence, Eqs. (4.8) and (4.10) yield Eqs. (2.6) and (2.7).

The fixed points and eigenvalues are listed in Table I. Using trace map (4.9) we establish the unphysical nature of fixed point no. 1 noting that $y^* = 0$. In fact, by exploiting the knowledge of the determinant [$\det(\mathbf{M}) = 1$] we find $\tilde{M}^{\,l}_{11} = x^* \pm [(x^*)^2 - 1]^{1/2}$. Since $\tilde{M}^{\,2}_{11}$ must be real, and $x^* = -\frac{1}{2}$, fixed point no. 1 is unphysical. Fixed point no.2 is reached for any $x_l = 0$. In fact, according to map (4.10), $x_l = 0$ implies $x_{l+1} = -1$ and $x_{l+\nu} = 1$ for any $\nu > 1$. From the equivalence of trace map (4.10) and the recursion relation of the characteristic polynomial (2.7) it then follows that all eigenvalues on the tree will lead to fixed point no. 2.

We also found a *period-2 cycle* $x_+^* \to x_-^* \to x_+^* \to \cdots$ with

$$x_\pm^* = -\frac{2R^2 + R + 1}{4R(R+1)} \pm \frac{1}{4R(R+1)}[(2R^2 + R + 1)^2 - 4(R+1)^2]^{1/2} , \tag{4.11}$$

where R is restricted to $-\frac{1}{2} > R > 1$. Besides these fixed points and period-2 solutions we have also found energy values yielding aperiodic behavior. All these typical different features of the maps are illustrated and compared in Fig. 8. Figure 8(a) shows the iterates for x_l, E_l, and U_l for $R = -0.5$ and an eigenvalue $E_{5,24} = 1.850\,781\,059\,358\,201\ldots$ leading to a fixed point no. 2. The number of iterates until the fixed point is reached is directly related to the level on the eigenvalue tree where the energy eigenvalue appears for the first time. The importance of the numerical accuracy is also demonstrated in this figure. Using double precision only, instead of extended precision (on an IBM-3081), numerical instability is already obtained after around 25 iterations. Figure 8(b) presents a period-2 cycle. There are two special choices of E and R such that the initial conditions lie on the fixed point, and no transient is required to reach the asymptotic behavior. They are given by

$$E = \xi_\pm, \quad R = \frac{\xi_\pm}{(2 + \xi_\pm - \xi_\pm^2)(1 - \xi_\pm)} , \tag{4.12}$$

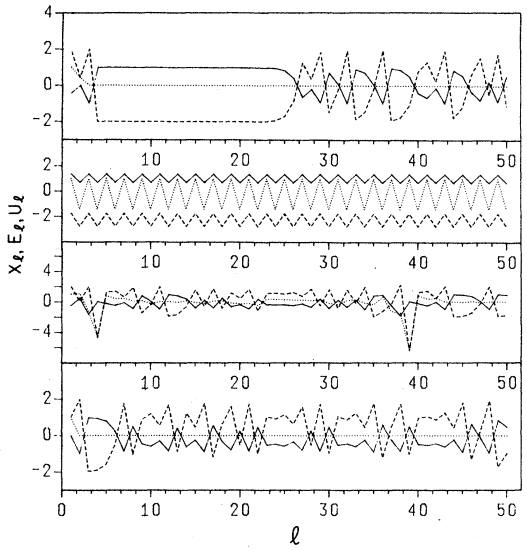

FIG. 8. Iterates of trace map x_l (solid curve) [Eq. (4.10)] and RG map E_l (dashed), U_l (dotted) [Eq. (3.2)] vs length l. (a) $R=-0.5$, and $E_0=1.850\,781\,059\,358\,201$, leading to fixed point no. 2 and becoming numerically unstable after approximately 25 itrations. (b) $R=-0.520\,072\,913\,415\,584\,086\,488\,9\ldots$ and $E_0=-1.741\,513\,025\,461\,326\,676\,19\ldots$, showing a cycle of period 2. (c) $R=-1.1$ and $E_0=1.988\,098\,03\ldots$, yielding an aperiodic sequence. (d) $R=0.5$ and $E_0=1.01$ for a bandlike state. In all cases $U_0=1$. Note that $2^{50}\simeq 10^{15}$. The lines are guides to the eye.

with

$$\xi_{\pm}=\tfrac{1}{2}\sqrt{u+5}\pm\tfrac{1}{2}[5-u+(u^2+4)^{1/2}]^{1/2}\ , \tag{4.13}$$

$$u=-\tfrac{1}{3}[(89+6\sqrt{318})^{1/2}+(89-6\sqrt{318})^{1/3}+5]\ .$$

The behavior of an *aperiodic* solution is shown in Fig. 8(c), for $R=-1.1$ and $E=1.988\,098\,03\ldots$, plotting X, U, and E. For completeness, we have examined a *bandlike* state for $R=0.5$ and $E=1.01$ in Fig. 8(d), as discussed in the previous section. Again, we obtain a disordered sequence for x_l and E_l, while U_l converges to 0. The positions of the fixed points and of period-2 cycles are illustrated in Fig. 9 as functions of R in the x-R plane. Fixed point no. 1 bifurcates at $R=1$, generating a period-2 cycle for $R>1$, as does fixed point no. 2 at $R=-\frac{1}{2}$. The crosses mark the position of the two analytically obtained period-2 cycles given in Eq. (4.13). Two other bifurcations occur at $R=-1$ and $\frac{1}{2}$, where fixed point no. 3 coincides with nos. 1 and 2, respectively.

Finally, we extend the analysis in terms of recursive relations to all elements of the transfer matrix M_l. From Eq. (4.9) we are already able to find two independent variables. Moreover, since $\det(M_l)=1$, only one more relation is required to evaluate the whole matrix. The simplest equation is found for $t_l\equiv M^l_{22}$:

$$t_l+1=2x_l t_l-1\ , \tag{4.14}$$

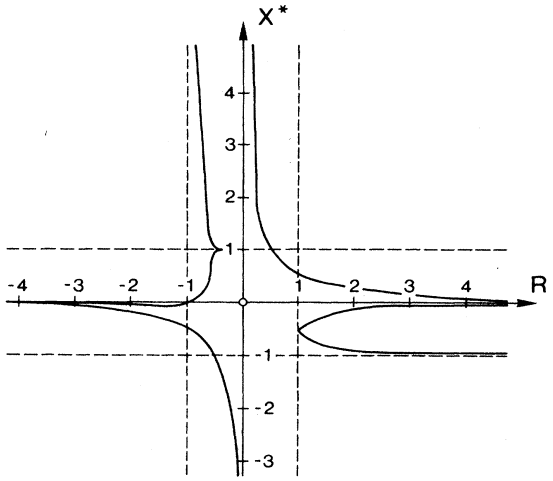

FIG. 9. R dependence of the fixed points x^* (Table I) including the period-2 solution [Eq. (4.11)].

with initial condition $t_0=0$. When analyzing the approach to fixed point no. 2, Eq. (4.14) is not sufficient to yield the entire dynamics, since $S_l=0$ does not allow determination of M^l_{12}. In such a case we must also add

$$\mathbf{M}^{l+1}_{12}=2x_l\mathbf{M}^l_{12}+\Lambda_l t_l+1 \tag{4.15}$$

with $M^0_{12}=-1$. More precisely, if we consider the eigenvalue $E_{l,\nu}$ at the $l=L$ hierarchy level, that is $x_{L-1}=0$, $x_L=-1$, $x_l=1$, we recognize that for $l>L$, $M^L_{12}=-\Lambda_L$, since $x_{L-1}=0$ and $t_L=-1$. Now we can derive an exact expression for the matrix elements M^{L+l}_{12}:

$$\begin{aligned}M^{L+l}_{12}&=2^l\Lambda_L\sum_{k=0}^{l}\left[\frac{R}{2}\right]^k\\&=R^{L-1}(R-1)\frac{2^{l+1}-R^{l+1}}{2-R},\quad |R|\neq 2\\&=R^{L-1}(R-1)2^l(l+1),\quad R=2\ .\end{aligned} \tag{4.16}$$

Since the matrix $\mathbf{M}^{L+l}$ relates the wave function $(\phi_{2^{L+l+1}},\phi_{2^{L+l}})$ to the initial pair (ϕ_1,ϕ_0) we can explicitly evaluate the scaling function on the sublattice points $2^{L+l}+1$ or 2^{L+l}, given by

$$\phi_{2^{L+l+1}}=\phi_1+M^{L+l}_{12}\phi_0,\ \phi_{2^{L+l}}=\phi_0\ . \tag{4.17}$$

It is worth noting that for $R=2$, Eq. (4.16) leads to logarithmic corrections to the scaling function.

V. PROPERTIES OF SHORT CHAINS

In experimental realizations, physical quantities for short systems are relevant and of particular interest. For this reason we consider the resistance ρ_N of systems of length N on the real lattice. It is defined as the ratio between total reflection and transmission coefficient τ_N and is given by[15,16]

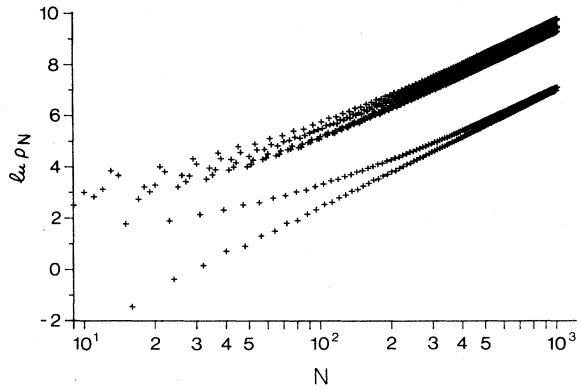

FIG. 10. N dependence of resistance $\ln\rho_N$ for $U_0=1$, $R=-\sqrt{3}/3$, $E=E_{3,3}=-1.600\,412\,735\,897\,52\ldots$.

$$\rho_N=\frac{1-\tau_N}{\tau_N}$$
$$=\frac{1}{4\sin^2\kappa}[\|M^N\|^2+2(M_{11}^N-M_{22}^N)(M_{12}^N-M_{21}^N)\cos\kappa$$
$$-4M_{12}^NM_{21}^N\cos^2\kappa-2]\ . \tag{5.1}$$

Here $E=2|E|_{\rm ex}\cos\kappa$, where $|E|_{\rm ex}$ denotes the maximum absolute energy value ($|R|\le 1$) of the spectrum and κ the wave number of the incident wave. $\|M^N\|$ is the Euclidean norm of the product of the transfer matrices up to site N (instead of 2^N as in the previous section). Besides the resistance and the transmission coefficient, we have also explored the behavior of the Euclidean norm $\|M^N\|$ and the trace of the matrix $\mathbf{M}^N$ on the real lattice as functions of energy and system size.

In Fig. 10 we show the natural logarithm of the resistance ρ_N versus the logarithm of length N for a system up to 1000 sites. The potential strength is $U_0=1$, $R=-\sqrt{3}/3$, and the energy value $E_{3,3}$ is the third eigenvalue on the third level of the eigenvalue tree. For this

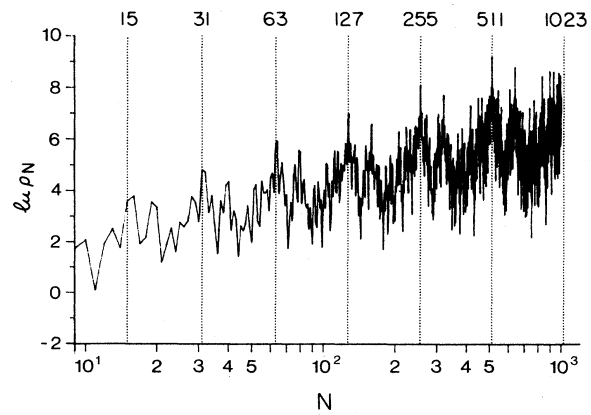

FIG. 11. N dependence of resistance $\ln\rho_N$ for $U_0=1$, $R=-\sqrt{3}/3$, $E=1-\sqrt{3}$.

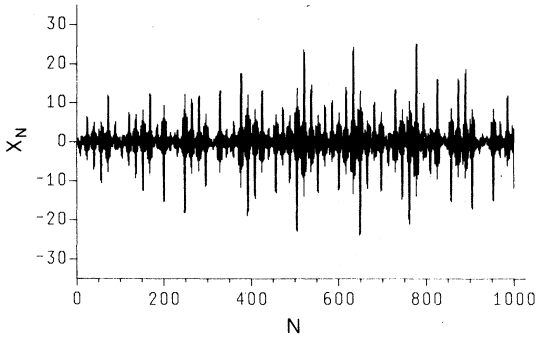

FIG. 12. N dependence of trace x_N for an aperiodic sequence with $U_0=1$, $R=-1.1$, $E=1.988\,098\,03\ldots$.

fixed point no. 2 solution, we get an algebraic increase with increasing length. On different sublattices we obtain different prefactors. The number of the prefactors 2^μ is determined by the level of the eigenvalue tree μ, to which the energy value belongs. The situation for a fixed point no. 3 solution, shown in Fig. 11, looks rather different. As an example we present the situation for the same potential strength $R=-\sqrt{3}/3$ and an energy value $E=1-\sqrt{3}$, which, in the spectrum, belongs to an integrated density of states of $\frac{1}{3}$. Superimposed on an average slope, we find a periodic structure exhibiting self-similar behavior. The peaks marked with the numbers 15,31,63, . . . , 511,1023 indicate the positions of the sublattice $n=2^l-1$. For the period-2 cycle, already discussed in the previous section, we obtain the same self-similar behavior for the resistance with, however, doubled period.

An aperiodic solution for $U_0=1$, $R=-1.1$, and $E=1.988\,098\,03\ldots$ is investigated in Fig. 12. To illustrate the behavior in this case we present the trace x_N as

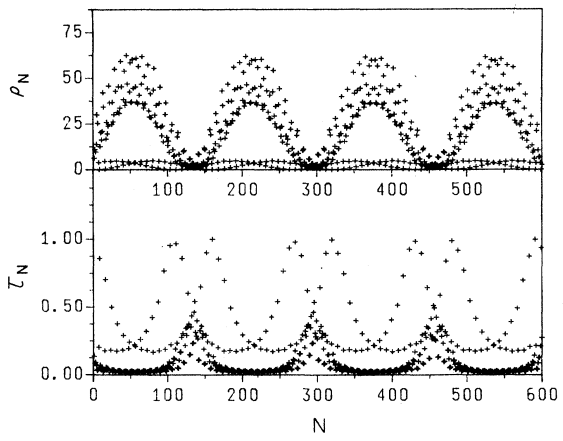

FIG. 13. N dependence of resistance ρ_N (upper part) and transmission τ_N (lower part) for a bandlike state with $U_0=1$, $R=-\sqrt{3}/3$, $E=-1.598$.

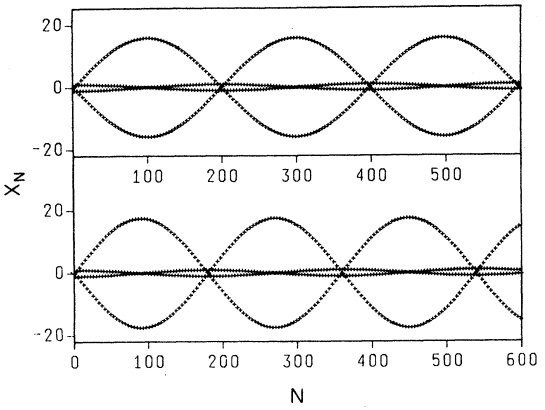

FIG. 14. N dependence of trace x_N for the ordered system with $U_0=1$, $R=1$, $E=1.001$ (upper curve) and for a bandlike state with $U_0=1$, $R=-\sqrt{3}$, $E=1.001$ (lower curve).

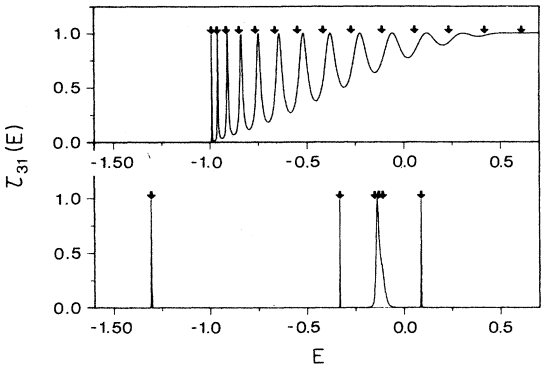

FIG. 15. Energy dependence of transmission τ_N for the ordered system of length $N=31$ with parameters $U_0=1$, $R=1$ (upper part) and for $U_0=1$, $R=-1$ (lower part). The arrows indicate the energetic position of the eigenvalues.

a function of length N. Irregular wild oscillations are the typical ingredients for energy values associated with aperiodic solution of the recursive map.

The bandlike behavior is discussed in the next two figures. Figure 13 shows the resistance ρ_N and transmission τ_N as a function of length N. The observed periodicity, in this case for parameters $U_0=1$, $R=-\sqrt{3}/3$, and $E=-1.598$, is typical for bandlike behavior. It is also remarkable that the transmission can change approximately by a factor 100 by increasing the system length by one more site. In Fig. 14 we compare the hierarchical case $R=-\sqrt{3}/3$ (lower part) with the completely ordered case $R=1$ (upper part) for an energy $E=1.001$ in the vicinity of the eigenvalue energy $E_{1,1}$ on the highest level. Other than a factor in the period length, the behavior is completely the same in both cases.

In the last figure we explore the energy dependence of the transmission coefficient τ_N. The upper part of Fig. 15 shows the ordered case for a system of length $N=31$. The transmission peaks $\tau_{31}(E)=1$ occur in the vicinity of the energy eigenvalues. The lower part of Fig. 15 illustrates the hierarchical case with $R=-1$. For this R value, in comparison to the periodic case, the transmission peaks are much less dense and considerably sharper. This behavior will become more pronounced for $|R|\to\infty$ because the eigenvalues appear in narrower clusters, as shown in Fig. 3.

VI. SUMMARY

To summarize, we have shown that the Schrödinger problem with hierarchical barrier structure reveals a very rich spectrum, as well as interesting resistance and transmission properties. Reducing the problem to recursion relations for the characteristic polynomials or to RG and trace maps, it became possible to determine and classify the energies belonging to the spectrum and identify scaling properties. We established that eigenvalues of the 2^l-1 system remain eigenvalues of the $2^{l+1}-1$ system, and new eigenvalues are created which split off from the old ones, yielding a tree structure. In terms of the RG and trace maps describing systems of $2^{l+1}-1$ or 2^L-1, respectively, iterations yield either bounded or exponentially growing iterates. Initial values leading to escape correspond to gap energies, while for *nonescaping* situations the initial value E_0 belongs to the spectrum, and can be classified as follows: (i) E_0 leads to a fixed point (all $E_0=E_\nu$ belonging to the tree lead to fixed point no. 2); (ii) E_0 yields periodic cycles (we found a cycle of period 2), and finally, (iii) an aperiodic motion is generated. Scaling properties of the spectrum and wave functions then follow from a linear stability analysis of such solution. Our numerical results confirm these predictions.

Thus, in contrast to periodic superlattices exhibiting gaps and bands only, a hierarchical array of barriers offers much richer properties. We hope that these new features can be observed experimentally and will turn out to be useful to tailor superlattices.

*Permanent address: Interdisziplinäres Projektzentrum für Supercomputing, Eidgenössiche Technische Hochschule -Zentrum, CH-8092 Zürich, Switzerland.

†Permanent address: Istituto Nazionale di Ottica, Largo Enrico Fermi 6, I-50125 Firenze, Italy.

‡Permanent address: Dipartimento di Fisica, Università di Salerno, I-84100 Salerno, Italy.

[1] B. Simon, Adv. Appl. Math. **3**, 463 (1982); J. B. Sokoloff, Phys. Rep. **126**, 189 (1985); G. Jona-Lasinio, F. Martinelli, and E. Scoppola, Ann. Inst. Henri Poincaré **42**, 73 (1985).

[2]M. Kohomoto, L. P. Kadanoff, and C. Tang, Phys. Rev. **50**, 1870 (1973); S. Ostlund, R. Paudit, D. Rand, H. J. Schellnhuber, and E. Siggia, Phys. Rev. Lett. **50**, 1873 (1983).
[3]L. Esaki, in *The Technology and Physics of Molecular Beam Epitaxy*, edited by E. H. C. Parker (Plenum, New York, 1985), p. 143.
[4]J. Todd, R. Merlein, R. Clarke, K. M. Mohanty, and J. D. Axe, Phys. Rev. Lett. **57**, 1157 (1986).
[5]R. Rammal and G. Toulouse, Rev. Mod. Phys. **58**, 765 (1986).
[6]K. H. Hoffmann, S. Grossmann, and F. Wegner, Z. Phys. **60**, 401 (1985).
[7]G. Mezard, G. Parisi, N. Sourlas, G. Toulouse, and M. Virasoro, Phys. Rev. Lett. **56**, 1156 (1984).
[8]D. Kutasov, A. Aharony, E. Domany, and W. Kinzel, Phys. Rev. Lett. **56**, 2229 (1986).
[9]R. H. Austin, K. W. Berson, L. Eisenstein, L. H. Frauenfelder, and I. C. Gunsalus, Biochem. **14**, 5355 (1975).
[10]B. A. Huberman and T. Hogg, Phys. Rev. Lett. **52**, 1084 (1984).
[11]T. Schneider, D. Würtz, A. Politi, and M. Zannetti, Phys. Rev. B **36**, 1789 (1987).
[12]P. Grassberger, R. Badii, and A. Politi (unpublished).
[13]T. Schneider, A. Politi, and D. Würtz, Z. Phys. B **60**, 469 (1987).
[14]H. G. Schuster, *Deterministic Chaos* (Physik-Verlag, Weinheim, 1984).
[15]L. Landauer, Philos. Mag. **21**, 863 (1970).
[16]A. D. Stone, J. D. Joannopoulos, and D. J. Chadi, Phys. Rev. B **24**, 5583 (1981).